Phase behaviors of cyclic diblock copolymers

Guojie Zhang, Zhongyong Fan, Yuliang Yang, and Feng Qiu

Citation: J. Chem. Phys. **135**, 174902 (2011); doi: 10.1063/1.3657437
View online: http://dx.doi.org/10.1063/1.3657437
View Table of Contents: http://jcp.aip.org/resource/1/JCPSA6/v135/i17
Published by the American Institute of Physics.

Phase behaviors of cyclic diblock copolymers

Guojie Zhang,[1,2] Zhongyong Fan,[2] Yuliang Yang,[1] and Feng Qiu[1,a)]
[1]*Key Laboratory of Molecular Engineering of Polymers, Key Laboratory of Computational Materials Science, Ministry of Education of China, Department of Macromolecular Science, Fudan University, Shanghai 200433, China*
[2]*Department of Materials Science, Fudan University, Shanghai 200433, China*

(Received 11 August 2011; accepted 11 October 2011; published online 3 November 2011)

A spectral method of self-consistent field theory has been applied to AB cyclic block copolymers. Phase behaviors of cyclic diblock copolymers, such as order-disorder transition, order-order transition, and domain spacing size, have been studied, showing good consistency with previous experimental and theoretical results. Compared to linear diblocks, cyclic diblocks are harder to phase separate due to the topological constraint of the ring structure. A direct disorder-to-cylinder transition window is observed in the phase diagram, which is significantly different from the mean field phase diagram of linear diblock copolymers. The domain spacing size ratio between cyclic and linear diblock copolymers is typically close to 0.707, indicating in segregation that the cyclic polymer can be considered to be made up of linear diblocks with half of the original chain length. © *2011 American Institute of Physics*. [doi:10.1063/1.3657437]

I. INTRODUCTION

Cyclic polymers, which are polymer chains with end segments being connected such that a ring is formed, are interesting materials with properties distinguished from linear polymers.[1] The promising properties of cyclic polymers essentially arise from their distinct conformational and dynamic properties in solution and melt states. Computer simulations have revealed that cyclic polymers adopt more compact conformations than their linear counterparts in melt state.[2–5] For example, the mean radii of gyration of cyclic polymers in melt state, R_g, scales with the molecular weight N as $R_g \propto N^{\nu}$ with $\nu \approx 0.39 \pm 0.03$.[2] This has been confirmed by recent experiments of small-angle neutron scattering for cyclic and linear poly(dimethylsiloxane) (PDMS), which showed that cyclic polymers indeed take more compact conformation: $R_g \propto N^{0.4}$ for cyclic PDMS, while $R_g \propto N^{0.5}$ for linear PDMS.[6] In solution, it was found that the hydrodynamic volume of cyclic polymers is smaller than that of their linear counterparts, leading to lower intrinsic viscosity.[7] The dynamic behaviors of cyclic polymers in melt are also distinctive. Cyclic polymers usually diffuse faster and their melt viscosity and plateau modulus are much lower than those of corresponding linear polymers.[3,4,8–10]

Block copolymers with cyclic architectures (cyclic block copolymers or block copolymer rings) only become a subject for study in recent years because of great difficulty in synthesis.[1,11] Cyclic block copolymers are copolymers with no chain end, i.e., a copolymer ring is formed in each polymer. With this ring architecture, AB cyclic block copolymers can only assume looped conformation in both disordered and phase-separated states, inducing remarkable differences in phase behaviors as compared to their linear counterparts.

It is expected that the order-disorder transition (ODT) will occur at larger χN for cyclic block copolymers than their linear counterparts, where χ is the Flory-Huggins parameter and N is the chain length. Mean-field theory with random phase approximation (RPA) showed that the critical point for cyclic diblock copolymer ($(\chi N)_c = 17.8$) is about 1.7 times larger than that for linear diblock ($(\chi N)_c = 10.5$).[12] Computer simulations also read larger $(\chi N)_{\mathrm{ODT}}$ for cyclic polymers due to the finite chain length used, e.g., $(\chi N)_{\mathrm{ODT}} = 45$ from dissipative particle dynamics (DPD) simulation[13] and $(\chi N)_{\mathrm{ODT}} = 42$ from Monte Carlo simulation.[14] Experiments on polystyrene-*b*-polyisoprene (PS-PI) diblock copolymers with PS volume fraction equaling 0.78 also showed a little larger $(\chi N)_{\mathrm{ODT}}$ for cyclic copolymers than the linear one.[15]

Cyclization of linear block copolymers usually results in morphological transformation both in melts and in solution.[15–18] Even if, with same chain length and composition, same phase structures are formed from linear and cyclic block copolymers, these phases always show different sizes of domain spacing.[12,14,16,19,20] For example, the ratio of domain spacing of a PS-PI cyclic copolymer and its linear copolymer was found to be 0.61.[20] Based on Leibler's theory and random-phase approximation, Marko predicted that the lamellar spacing ratio of a cyclic to its corresponding diblock copolymer is about 0.67 in the weak segregation limit and about 0.63 in the strong segregation limit.[12] Monte Carlo simulations also concluded that the ratio of the domain spacing between the cyclic diblock copolymer and the corresponding linear diblock is 0.7.[14]

Although advances in synthesis and phase behavior of cyclic block copolymers have been achieved, a full understanding of its equilibrium behavior is far from reach. Theoretical phase diagram, especially based on self-consistent field theory (SCFT), of AB cyclic diblock copolymers is still absent. In this paper, we use SCFT to calculate the phase diagram of AB cyclic diblock copolymers.

a)Author to whom correspondence should be addressed. Electronic mail: fengqiu@fudan.edu.cn.

SCFT has been one of the most successful theories for description of equilibrium behaviors of inhomogeneous polymers.[21] Its application covers a wide range from block copolymers to polymer blends, concentrated polymer solution, polymer brush etc. In SCFT, the key elements are to calculate the single chain partition function and chain propagator, in terms of which almost all thermodynamic properties (such as free energy) and thus phase behaviors can be determined.[21] For non-cyclic polymers, including linear, star-shaped, comb-like copolymers, etc, end-integrated chain propagators are defined and are sufficient for description of topologies of these polymers. For cyclic polymers, however, non-end-integrated chain propagators must be introduced for accurately describing the cyclic topology. As a consequence, additional degrees of freedom, leading to much more computational cost if the SCFT equations are solved in real space, are emerged. Therefore, more efficient numerical method is needed in case of cyclic polymers. Here, we adopt the spectral method,[22] which has been proven to be a powerful approach in accurate calculation of thermodynamic properties. We will show that the additional degrees of freedom can be analytically integrated out in spectral method, leading to almost the same computational cost for cyclic polymers as for linear polymers. Using the spectral method, we have established phase diagram of AB cyclic diblock copolymers. Distinct features of cyclic block copolymers in terms of ODT and domain spacing size are also discussed.

II. THEORY

The model system consists of n AB cyclic diblock copolymers with polymer length N in volume V. The A monomer volume fraction is f. We assume that the A- and B-monomer have the same volume, $1/\rho_0$, and also the same statistical segment length, b. The conformation of the ith chain is described by a space curve, $\mathbf{R}_i(s)$, $s \in [0, 1]$. Then, the partition function in canonical ensemble is written as

$$Z \sim \int D\{\mathbf{R}(\bullet)\} P\{\mathbf{R}(\bullet)\} \delta[1-\hat{\phi}_{\mathrm{A}}-\hat{\phi}_{\mathrm{B}}] \exp[-W/k_{\mathrm{B}}T], \tag{1}$$

with

$$P\{\mathbf{R}(\bullet)\} = \prod_i \exp\left[-\frac{3}{2Nb^2}\int_0^1 \mathrm{d}s \left(\frac{\mathrm{d}\mathbf{R}_i(s)}{\mathrm{d}s}\right)^2\right], \tag{2}$$

where $\mathbf{R}(\bullet) \equiv \{\mathbf{R}_1(\bullet), \mathbf{R}_2(\bullet), \ldots, \mathbf{R}_n(\bullet)\}$ ($\mathbf{R}_i(\bullet)$ represents the conformation of the ith chain) denotes the chain configuration. The last term in Eq. (1), W, is the contribution from monomer interactions, and $W = k_{\mathrm{B}}T\chi\rho_0 \int \mathrm{d}\mathbf{r}\hat{\phi}_{\mathrm{A}}(\mathbf{r})\hat{\phi}_{\mathrm{B}}(\mathbf{r})$, where χ is the Flory-Huggins parameter. The segment density operator $\hat{\phi}_{\mathrm{A}}(\mathbf{r})$ is defined as

$$\hat{\phi}_{\mathrm{A}}(\mathbf{r}) = \frac{N}{\rho_0}\sum_{i=1}^{n}\int_0^f \mathrm{d}s\,\delta(\mathbf{r}-\mathbf{R}_i(s)). \tag{3}$$

and $\hat{\phi}_{\mathrm{B}}(\mathbf{r})$ has similar definition with s ranging from f to 1. After taking the particle-to-field transformation,[21] external fields $\omega_{\mathrm{A}}(\mathbf{r})$ and $\omega_{\mathrm{B}}(\mathbf{r})$ conjugated, respectively, to the density fields $\phi_{\mathrm{A}}(\mathbf{r})$ and $\phi_{\mathrm{B}}(\mathbf{r})$ are introduced, then the partition function is expressed as a functional integral of the density and external fields,

$$Z \sim \int D\{\phi\} D\{\omega\} \exp[-F(\{\phi\},\{\omega\})/k_{\mathrm{B}}T], \tag{4}$$

where the functional F is represented as

$$F(\{\phi\},\{\omega\}) = \frac{\rho_0 R_g^3 k_{\mathrm{B}}T}{N}\left\{-V\ln Q + \int \mathrm{d}\mathbf{r}\left[\chi N\phi_{\mathrm{A}}(\mathbf{r})\phi_{\mathrm{B}}(\mathbf{r}) - \omega_{\mathrm{A}}(\mathbf{r})\phi_{\mathrm{A}}(\mathbf{r}) - \omega_{\mathrm{B}}(\mathbf{r})\phi_{\mathrm{B}}(\mathbf{r})\right]\right\}. \tag{5}$$

The single-chain partition function Q is given as

$$Q = \frac{1}{V}\int D(\mathbf{R}_i(s)) P(\mathbf{R}_i(s)) \exp\left[-\int_0^1 \mathrm{d}s\,\omega(\mathbf{R}_i(s))\right]. \tag{6}$$

For mathematical convenience, forward and backward chain propagators are defined, respectively, as

$$q(\mathbf{r}, s|\mathbf{r}_0) \equiv \int D\{\mathbf{R}(\bullet)\} P\{\mathbf{R}(\bullet)\} \times \exp\left[-\sum_\alpha \int_0^s \mathrm{d}t\,\omega_\alpha(\mathbf{R}(t))\gamma_\alpha(t)\right] \times \delta(\mathbf{r}-\mathbf{R}(s))\delta(\mathbf{r}_0-\mathbf{R}(0)), \tag{7}$$

$$q^\dagger(\mathbf{r}, s|\mathbf{r}_0) \equiv \int D\{\mathbf{R}(\bullet)\} P\{\mathbf{R}(\bullet)\} \times \exp\left[-\sum_\alpha \int_s^1 \mathrm{d}t\,\omega_\alpha(\mathbf{R}(t))\gamma_\alpha(t)\right] \times \delta(\mathbf{r}-\mathbf{R}(s))\delta(\mathbf{r}_0-\mathbf{R}(1)), \tag{8}$$

in which the type of monomer α is constrained by $\gamma_\alpha(t)$, $\alpha = \mathrm{A}, \mathrm{B}$, with

$$\gamma_\alpha(t) = \delta_{\mathrm{A},\alpha}\, t \in (0, f),$$

$$\gamma_\alpha(t) = \delta_{\mathrm{B},\alpha}\, t \in (f, 1).$$

The second δ-functions in Eqs. (7) and (8) ensure the cyclic structure of the block copolymer. With these definitions, the partition function can be written as

$$Q = \frac{1}{V}\int \mathrm{d}\mathbf{r}\int \mathrm{d}\mathbf{r}_0 q(\mathbf{r}, s|\mathbf{r}_0) q^\dagger(\mathbf{r}, s|\mathbf{r}_0). \tag{9}$$

Obviously, the two chain propagators obey the following modified diffusion equations:

$$\frac{\partial}{\partial s}q(\mathbf{r}, s|\mathbf{r}_0) = R_g^2\nabla^2 q(\mathbf{r}, s|\mathbf{r}_0) - \omega(\mathbf{r}) q(\mathbf{r}, s|\mathbf{r}_0), \tag{10}$$

$$\frac{\partial}{\partial s}q^\dagger(\mathbf{r}, s|\mathbf{r}_0) = -R_g^2\nabla^2 q^\dagger(\mathbf{r}, s|\mathbf{r}_0) + \omega(\mathbf{r}) q^\dagger(\mathbf{r}, s|\mathbf{r}_0). \tag{11}$$

For cyclic copolymers considered here, the initial conditions for the above modified diffusion equations are

$$q\left(\mathbf{r}, 0\left|\mathbf{r}_0\right.\right)=\delta\left(\mathbf{r}-\mathbf{r}_0\right), \quad q^{\dagger}\left(\mathbf{r}, 1\left|\mathbf{r}_0\right.\right)=\delta\left(\mathbf{r}-\mathbf{r}_0\right), \tag{12}$$

where $\mathbf{r}_0$ is the spatial coordinate of the segment that connects the head ($s=0$) and tail ($s=1$) in a cyclic chain. Then, the above two equations should be solved under sets of initial conditions where $\mathbf{r}_0 \in \Omega$, Ω denote the computational space (with its volume equal to V).

By mean-field approximation, obtained are the following (SCFT) equations:

$$\phi_{\mathrm{A}}\left(\mathbf{r}\right)=\frac{1}{Q}\int_0^f \mathrm{d}s\int \mathrm{d}\mathbf{r}_0 q\left(\mathbf{r}, s\left|\mathbf{r}_0\right.\right) q^{\dagger}\left(\mathbf{r}, s\left|\mathbf{r}_0\right.\right), \tag{13}$$

$$\phi_{\mathrm{B}}\left(\mathbf{r}\right)=\frac{1}{Q}\int_f^1 \mathrm{d}s\int \mathrm{d}\mathbf{r}_0 q\left(\mathbf{r}, s\left|\mathbf{r}_0\right.\right) q^{\dagger}\left(\mathbf{r}, s\left|\mathbf{r}_0\right.\right), \tag{14}$$

$$\omega_{\mathrm{A}}(\mathbf{r})=\chi N\phi_{\mathrm{B}}(\mathbf{r})+\eta(\mathbf{r}), \tag{15}$$

$$\omega_{\mathrm{B}}(\mathbf{r})=\chi N\phi_{\mathrm{A}}(\mathbf{r})+\eta(\mathbf{r}), \tag{16}$$

$$\phi_{\mathrm{A}}(\mathbf{r})+\phi_{\mathrm{B}}(\mathbf{r})=1. \tag{17}$$

It is obvious from Eqs. (10)–(17) that the additional degree of freedom, $\mathbf{r}_0$, would cause significantly larger computational cost when numerically solved in real space. This has made the real-space method impractical in dealing with cyclic chains.[23]

Here, we solve the SCFT equations with the spectral method[22] which will be proven an optimal method for SCFT of cyclic polymers. Specifically, in the spectral method, any spatially varying function is expanded as orthonormal basis functions which have certain symmetries being considered. For example, the chain propagator $q\left(\mathbf{r}, s\left|\mathbf{r}_0\right.\right) = \sum_j q_j(s\left|\mathbf{r}_0\right.) f_j(\mathbf{r})$, where $V^{-1}\int f_i(\mathbf{r}) f_j(\mathbf{r}) d\mathbf{r} = \delta_{ij}$ and $\nabla^2 f_i(\mathbf{r}) = -\lambda_i D^{-2} f_i(\mathbf{r})$, $f_i(\mathbf{r})$ is the basis function and D is the length scale (in unit of R_g) of the computational box. The basis functions are arranged such that λ_i is listed in an increasing way with $\lambda_1 = 0$. Then, differential equations (10) and (11) can be expressed as

$$\frac{\partial q_i(s\left|\mathbf{r}_0\right.)}{\partial s}=-\sum_j H_{ij} q_j(s\left|\mathbf{r}_0\right.), \tag{18}$$

$$\frac{\partial q_i^{\dagger}(s\left|\mathbf{r}_0\right.)}{\partial s}=\sum_j H_{ij} q_j^{\dagger}(s\left|\mathbf{r}_0\right.), \tag{19}$$

with initial conditions

$$q_j\left(0\left|\mathbf{r}_0\right.\right)=f_j\left(\mathbf{r}_0\right)/V, \quad q_j^{\dagger}\left(1\left|\mathbf{r}_0\right.\right)=f_j\left(\mathbf{r}_0\right)/V. \tag{20}$$

The Hamiltonians are

$$H_{ij}=\lambda_i D^{-2}\delta_{\mathbf{G}_i,\mathbf{G}_j}+\sum_k \omega_{\alpha,k}(s)\Gamma_{ijk}, \tag{21}$$

$$\Gamma_{ijk}=\frac{1}{V}\int f_i(\mathbf{r}) f_j(\mathbf{r}) f_k(\mathbf{r}) d\mathbf{r}. \tag{22}$$

In the same way, segment density fields and external fields are expressed as

$$\phi_{\mathrm{A}}\left(\mathbf{r}\right)=\sum_i \phi_{\mathrm{A},i} f_i\left(\mathbf{r}\right); \phi_{\mathrm{B}}\left(\mathbf{r}\right)=\sum_i \phi_{\mathrm{B},i} f_i\left(\mathbf{r}\right),$$

$$\omega_{\mathrm{A}}\left(\mathbf{r}\right)=\sum_i \omega_{\mathrm{A},i} f_i\left(\mathbf{r}\right); \omega_{\mathrm{B}}\left(\mathbf{r}\right)=\sum_i \omega_{\mathrm{B},i} f_i\left(\mathbf{r}\right).$$

The solutions of the above ordinary differential equations (18) and (19) become

$$q_i\left(s\left|\mathbf{r}_0\right.\right)=\begin{cases}\sum_j T_{\mathrm{A},ij}\left(s\right) q_j\left(0\left|\mathbf{r}_0\right.\right), & s\in(0,\, f)\\ \sum_j T_{\mathrm{B},ij}\left(s-f\right) q_j\left(f\left|\mathbf{r}_0\right.\right), & s\in(f,\, 1)\end{cases}, \tag{23}$$

$$q_i^{\dagger}\left(s\left|\mathbf{r}_0\right.\right)=\begin{cases}\sum_j T_{\mathrm{B},ij}\left(1-s\right) q_j^{\dagger}\left(1\left|\mathbf{r}_0\right.\right), & s\in(f,\, 1)\\ \sum_j T_{\mathrm{A},ij}\left(f-s\right) q_j^{\dagger}\left(f\left|\mathbf{r}_0\right.\right), & s\in(0,\, f)\end{cases}, \tag{24}$$

where T_{ij} is the element of matrix $\mathbf{T}$, and $\mathbf{T}(s) = \exp\left[\mathbf{H}s\right]$. The single-chain partition function is given as

$$Q=\int \mathrm{d}\mathbf{r}_0 \sum_i q_i\left(s\left|\mathbf{r}_0\right.\right) q_i^{\dagger}\left(s\left|\mathbf{r}_0\right.\right), \text{ for } \forall s. \tag{25}$$

The coefficients for density fields are represented as

$$\phi_{\mathrm{A},i}=\frac{1}{Q}\int_0^f \mathrm{d}s\int \mathrm{d}\mathbf{r}_0 \sum_j\sum_k q_j\left(s\left|\mathbf{r}_0\right.\right) q_k^{\dagger}\left(s\left|\mathbf{r}_0\right.\right)\Gamma_{ijk}, \tag{26}$$

$$\phi_{\mathrm{B},i}=\frac{1}{Q}\int_f^1 \mathrm{d}s\int \mathrm{d}\mathbf{r}_0 \sum_j\sum_k q_j\left(s\left|\mathbf{r}_0\right.\right) q_k^{\dagger}\left(s\left|\mathbf{r}_0\right.\right)\Gamma_{ijk}. \tag{27}$$

More specifically, after expressing the matrix $\mathbf{T}$ in terms of its eigenvectors $\mathbf{U}$ (its element is denoted as U_{ij}) and eigenvalues $\mathbf{D}$ (its element is denoted as d_i), $\mathbf{T} = \mathbf{U}\exp\left[-\mathbf{D}s\right]\mathbf{U}^{\dagger}$, the density fields are given as

$$\phi_{\mathrm{A},i}=\frac{1}{VQ}\sum_j\sum_k\Gamma_{ijk}\sum_a\sum_b\sum_c\sum_d\sum_e U_{\mathrm{A},jc}U_{\mathrm{A},kd}U_{\mathrm{B},be} U_{\mathrm{A},ca}^T U_{\mathrm{A},db}^T U_{\mathrm{B},ea}^T \frac{e^{-d_{\mathrm{A},c}f}-e^{-d_{\mathrm{A},d}f}}{d_{\mathrm{A},d}-d_{\mathrm{A},c}} e^{-d_{\mathrm{B},e}(1-f)}, \tag{28}$$

$$\phi_{\mathrm{B},i}=\frac{1}{VQ}\sum_j\sum_k\Gamma_{ijk}\sum_a\sum_b\sum_c\sum_d\sum_e U_{\mathrm{B},jb}U_{\mathrm{B},kd}U_{\mathrm{A},ae} U_{\mathrm{B},dc}^T U_{\mathrm{B},ba}^T U_{\mathrm{A},ec}^T \frac{e^{-d_{\mathrm{B},b}(1-f)}-e^{-d_{\mathrm{B},d}(1-f)}}{d_{\mathrm{B},d}-d_{\mathrm{B},b}} e^{-d_{\mathrm{A},e}f}, \tag{29}$$

$$Q = \frac{1}{V}\sum_i \sum_j U_{\mathrm{A},ij} \exp(-d_{\mathrm{A},j} f) U^T_{\mathrm{A},ji}. \quad (30)$$

The free energy can be written as

$$\frac{F}{nk_\mathrm{B}T} = -\ln Q - \chi N \sum_i \phi_{\mathrm{A},i}\phi_{\mathrm{B},i}. \quad (31)$$

The coefficients for external field are determined self-consistently:

$$\omega_{\mathrm{A},i} = \chi N \phi_{\mathrm{B},i} + \eta_i,$$

$$\omega_{\mathrm{B},i} = \chi N \phi_{\mathrm{A},i} + \eta_i,$$

$$\phi_{\mathrm{A},i} + \phi_{\mathrm{B},i} = \delta_{i1}.$$

It can be seen that segment density coefficients (Eqs. (28) and (29)) are also expressed in terms of eigenvectors and eigenvalues of the Hamiltonian as in case of linear diblock copolymers.[22] Therefore, no additional computational cost is induced for cyclic diblock copolymers.

For establishing phase diagram of cyclic diblock copolymers, five candidate phases are considered: disordered, lamellae, hexagonally arranged cylinders, body-centered cubic sphere, and gyroid. Then the stable phases are obtained as the phases with minimum free energy with respect to D (the length scale of computational box) for any molecular parameters (f, χN).

III. RESULTS AND DISCUSSION

A. Phase diagram

The calculated phase diagram of AB cyclic diblock copolymers is shown in Fig. 1, where lamellae (L), hexagonal cylinder (C), body-centered-cubic sphere (S), gyroid (G), and disordered phase (D) are considered as candidates. Due to large number of basis functions needed in very strong segregation region, we calculated the phase diagram only up to $\chi N = 80$, and C-G and G-L phase boundaries are not actually determined for $40 \le \chi N \le 80$ for the same reason. We just simply extrapolate these phase boundaries from $\chi N = 40$ to 80. Note that 130 basis functions are used during the SCFT calculations. It appears that the shape of the phase diagram is similar to the linear one. Nevertheless, there are several features that distinguish it from the phase diagram of linear diblock copolymers. Firstly, $(\chi N)_{\mathrm{ODT}}$ for cyclic diblocks is significantly larger than the corresponding linear one. For example, the critical point for cyclic diblock is $\chi N = 15.7$ and that for linear diblock is $\chi N = 10.5$. Secondly, the sphere phases end at triple points: $\chi N = 24.1$ with $f = 0.275$ and 0.725. Thus, there is a large compositional window (f: 0.275–0.725) through which direct disorder-to-cylinder transition occurs. Such window does not exist in the phase diagram of linear diblock copolymers. Finally, the phase diagram of cyclic diblock copolymers seems "thinner" than that of the linear one, which means stronger interaction parameter in cyclic diblocks is necessary to exhibit the same microphase-separation behavior as in linear diblocks with the same composition.

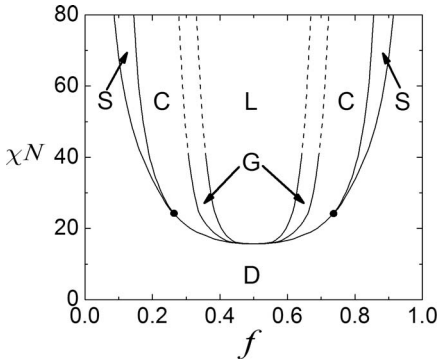

FIG. 1. SCFT phase diagram of AB cyclic diblock copolymers, in which phase boundaries of lamellae (L), hexagonal cylinder (C), gyroid (G), body-centered-cubic sphere (S), and disorder (D) are shown. χ is the Flory-Huggins parameter, N is the polymerization index of block copolymers, and f is the volume fraction of A monomer in the system.

Up to now, although experimental studies on phase behaviors of cyclic diblock copolymers have been carried out for years, they are limited to few cases, including polystyrene-*b*-poly(dimethylsi1oxane),[19] polyisoprene-*b*-polystyrene (PI-PS),[24] and polystyrene-*b*-polybutadiene (PS-PBD).[16] More importantly, owning to limited compositional versatility of cyclic diblock copolymers studied, only three ordered phases (lamellae, cylinder, and sphere) have been observed. The lamellae phase is always found in near symmetric cyclic diblock copolymers ($f = 0.48$–0.53),[16,19,24,25] except a PS-PBD cyclic copolymer with $f = 0.378$.[16] Considering that the χN values of the PS-PBD cyclic diblock copolymers under investigation are in range of 52–81 at room temperature and 40–61 at the sample annealing temperature,[16] the observed lamellae phase with $f = 0.378$ for PS-PBD is justified according to our SCFT phase diagram. For cylinder structure, the volume fraction of the samples is located at 0.24 (Ref. 16) and 0.30 (Ref. 24) for PS-PBD and PI-PS, respectively, which could be deduced from the SCFT phase diagram. The experimental results showed that the sphere phase is observed at $f = 0.13$ and 0.108 for PI-PS (Ref. 24) and PS-PBD (Ref. 16) cyclic diblock copolymers, respectively. It is obvious from the SCFT phase diagram that the $(\chi N)_{\mathrm{ODT}}$ (corresponding to disorder-to-sphere transition) at these two volume fractions are 52.1 and 62.9, respectively. Therefore, we can expect if the χN values of the PI-PS and PS-PBD cyclic diblocks are greater than 52.1 and 62.9, respectively, sphere phase should be observed. This expectation is supported by the experiment since the calculated $(\chi N)_{\mathrm{ODT}}$ falls into the estimated χN region of the PS-PBD cyclic diblocks where sphere phase occurred.[16]

The phase diagram from SCFT calculation can also be compared to those from Leibler's theory[26] and DPD simulations.[13] Morozov *et al.* calculated the phase diagram of AB cyclic diblock copolymers via Leibler's mean field theory, which is in qualitative agreement with our results. In its phase diagram, a composition window ($f = 0.33$–0.67) of direct transition from disordered phase to cylinders was also found. The notable difference between the phase diagrams from Leibler's theory and SCFT is that the $(\chi N)_{\mathrm{ODT}}$

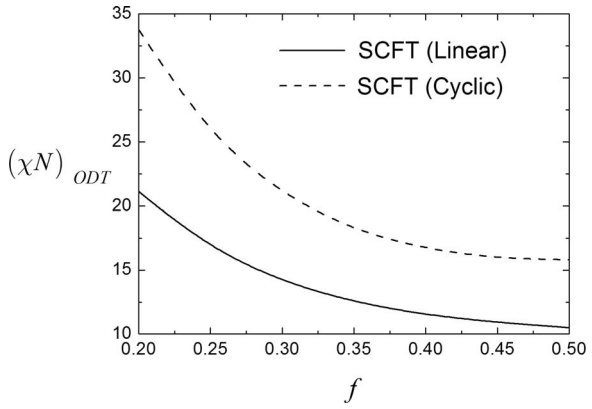

FIG. 2. Order-disorder transitions (ODT) of cyclic and linear diblock copolymers from SCFT calculation.

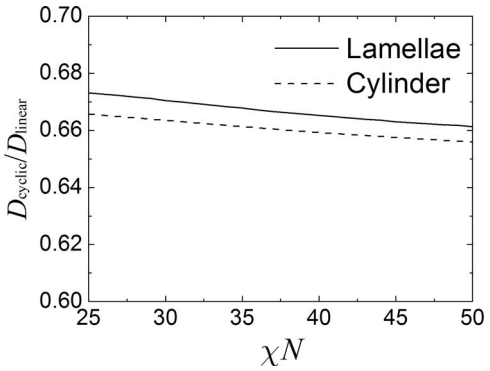

FIG. 3. Influence of χN upon domain spacing ratio of AB cyclic block copolymers and corresponding linear diblock copolymers in melts.

for the former is higher than the latter. Based on DPD simulations, Qian *et al*. also reported a phase diagram of cyclic copolymers.[13] In their results, the stable morphologies included lamellae, perforated lamellae, hexagonally arranged cylinders, and spheres. They also found that a direct disorder-to-cylinder transition occurs at $0.2 < f < 0.35$. Note that significantly larger $(\chi N)_{\mathrm{ODT}}$ values in their phase diagram might be due to the finite chain length used in their DPD simulations.

B. Order-disorder transition

Figure 2 compared the ODT behavior of cyclic and linear diblocks. It can be seen that the $(\chi N)_{\mathrm{ODT}}$ line of cyclic diblock copolymers always stays above that of linear diblock copolymers, indicating that cyclic copolymers need stronger segregation (larger χN or lower temperature in most cases) than linear copolymers to be phase-separated. In a cyclic chain, the two blocks are connected with two junctions rather than only one in linear block copolymers. This topological constraint makes the two block subchains in cyclic diblocks closer neighbors that are harder to be phase-separated, therefore stronger repulsive interaction is needed.

C. Domain size

Near the G-L transition, the ratio of domain sizes of G phase to L phase, $D_{\mathrm{G}}/D_{\mathrm{L}}$, is ranging from 2.47 to 2.40 when χN is increasing from 18 to 40. Note that it is almost the same value for the ratio in AB linear diblock copolymers.[22] This result implies that cyclic topology of diblock copolymers makes no significant difference on the ratio of characteristic sizes of different phases, although it certainly affects their characteristic sizes themselves. Other values for such ratio are $D_{\mathrm{G}}/D_{\mathrm{C}} = 2.15$–$2.19$ for $\chi N = 18$–40, and $D_{\mathrm{S}}/D_{\mathrm{C}} = 1.21$–$1.15$ for $\chi N = 27$–80. We note that these theoretical predictions need experimental verifications in the future.

It is expected that cyclization of linear block copolymers can lead to different structural behaviors. Experimental and theoretical results have concluded that the domain spacing size of cyclic copolymers is smaller than their linear counterpart due to the molecular architecture of cyclic polymers.[12,14,16,19,20,24] Figure 3 shows domain spacing size ratio between cyclic and linear diblock copolymers, where lamellae and cylinder phase are considered. It appears that domain spacing ratios for both phases are near 0.67, decreasing slightly with increasing χN. Note that theoretical prediction from RPA gives the ratio as 0.67 in weak segregation limit, which decreases to 0.63 in strong segregation limit.[12] Experimental results also confirm this conclusion.[20] The smaller domain size of cyclic block copolymers is readily explained. In any phase-separated structures, AB cyclic copolymers should adopt only loop conformation due to their ring architecture. For AB linear diblocks, however, only bridge conformation is valid. Consequently, the effective chain length of cyclic copolymers seems to be shortened to almost half of the corresponding AB linear polymers, leading to $R_{g,\mathrm{linear}} = \sqrt{2}R_{g,\mathrm{cyclic}}$. Then, the domain size ratio of cyclic to linear diblock copolymer is about $R_{g,\mathrm{cyclic}}/R_{g,\mathrm{linear}} = 1/\sqrt{2} \approx 0.707$, as compared to the RPA prediction, 0.67. ABA linear triblock copolymers stand as an intermediate one, in which both loop and bridge conformations are allowed, resulting in almost the same domain size as their corresponding cyclic chains.[24]

D. Conformational statistics

It is well known that the chain conformation plays an important role in physical properties of polymeric materials. Therefore, it is necessary to illuminate conformational behaviors of cyclic polymers in melt and solution states. In disordered melt state, conclusion has been made from both experiment and simulations that cyclic polymers show more compact conformation than linear polymers.[2–6] In phase-separated states, however, the conformational characteristic of cyclic block copolymers is not clear. Due to topological distinction, we expect that there is a different conformational feature for cyclic block copolymers. Monte Carlo simulation results show that cyclic diblock copolymers in lamellar phase are strongly stretched perpendicularly to the interface.[27] With decreasing temperature, the radius of the mass center of two blocks in cyclic copolymers increases by about 20%–25%, while the end-to-end vector of the blocks decreases by almost 15%.[27] As a comparison with the Monte Carlo simulations, we also define the end-to-end distance of the two blocks in

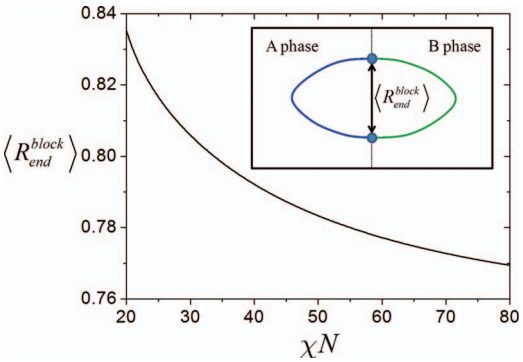

FIG. 4. The effect of χN on the end-to-end distance of the two blocks (in unit of R_g) for a symmetric cyclic diblock. The inset sketches the end-to-end distance of the two blocks.

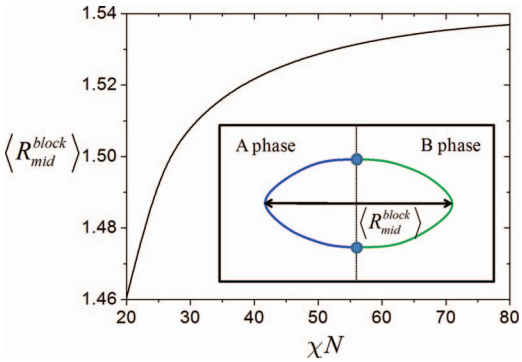

FIG. 5. The effect of χN on the middle-segments distance of the two blocks (in unit of R_g) for a symmetric cyclic diblock. The inset sketches the middle-segments distance of the two blocks.

the framework of SCFT as following:

$$\langle R_{\text{end}}^{\text{block}} \rangle = \left[\frac{\int d\mathbf{r} \int d\mathbf{r}_0 q(\mathbf{r}, f|\mathbf{r}_0) q^{\dagger}(\mathbf{r}, f|\mathbf{r}_0)(\mathbf{r}-\mathbf{r}_0)^2}{\int d\mathbf{r} \int d\mathbf{r}_0 q(\mathbf{r}, f|\mathbf{r}_0) q^{\dagger}(\mathbf{r}, f|\mathbf{r}_0)} \right]^{1/2}. \tag{32}$$

For simplicity, only lamellar phase of symmetric cyclic diblock copolymers ($f = 0.50$) is investigated as in the Monte Carlo simulation.[27] In addition to the end-to-end distance, the distance of two middle segments of the two blocks can be defined as

$$\langle R_{mid}^{\text{block}} \rangle = \left[\frac{\int d\mathbf{r} \int d\mathbf{r}_0 q(\mathbf{r}, f/2|\mathbf{r}_0) q^{\dagger}(\mathbf{r}, f/2|\mathbf{r}_0)(\mathbf{r}_{\perp}-\mathbf{r}_{0,\perp})^2}{\int d\mathbf{r} \int d\mathbf{r}_0 q(\mathbf{r}, f/2|\mathbf{r}_0) q^{\dagger}(\mathbf{r}, f/2|\mathbf{r}_0)} \right]^{1/2}$$
$$+ \left[\frac{\int d\mathbf{r} \int d\mathbf{r}_0 q(\mathbf{r}, (1+f)/2|\mathbf{r}_0) q^{\dagger}(\mathbf{r}, (1+f)2|\mathbf{r}_0)(\mathbf{r}_{\perp}-\mathbf{r}_{0,\perp})^2}{\int d\mathbf{r} \int d\mathbf{r}_0 q(\mathbf{r}, (1+f)2|\mathbf{r}_0) q^{\dagger}(\mathbf{r}, (1+f)/2|\mathbf{r}_0)} \right]^{1/2}. \tag{33}$$

For lamellar phase of symmetric cyclic diblock copolymers, Eq. (33) is simplified as

$$\langle R_{mid}^{\text{block}} \rangle = 2 \left[\frac{\int d\mathbf{r} \int d\mathbf{r}_0 q(\mathbf{r}, 1/4|\mathbf{r}_0) q^{\dagger}(\mathbf{r}, 1/4|\mathbf{r}_0)(\mathbf{r}_{\perp}-\mathbf{r}_{0,\perp})^2}{\int d\mathbf{r} \int d\mathbf{r}_0 q(\mathbf{r}, 1/4|\mathbf{r}_0) q^{\dagger}(\mathbf{r}, 1/4|\mathbf{r}_0)} \right]^{1/2}, \tag{34}$$

where $\mathbf{r}_{\perp}$ and $\mathbf{r}_{0,\perp}$ are the spatial position of the middle segment and the junction segment of blocks along axis perpendicular to the interface of lamellae, respectively. The effects of interaction parameter χN on the conformation characteristics $\langle R_{\text{end}}^{\text{block}} \rangle$ and $\langle R_{mid}^{\text{block}} \rangle$ are shown in Figs. 4 and 5, respectively. It is found that $\langle R_{\text{end}}^{\text{block}} \rangle$ decreases by about 10% with increasing χN from 20 to 80, while $\langle R_{mid}^{\text{block}} \rangle$ increases by about 7%. These findings indicate that stretched chain conformation is formed in phase-separated states of cyclic block copolymers, which is in qualitative agreement with the results of Monte Carlo simulation.[27]

IV. SUMMARY

We have calculated the phase diagram for AB cyclic block copolymers based on self-consistent field theory. A spectral method was adopted to achieve accuracy and efficiency. Phase behaviors of cyclic block copolymers, such as order-disorder transition, order-order transition, domain spacing size, have been studied, showing good consistency with previous experimental and theoretical results. Compared to linear diblock copolymers, cyclic diblocks are harder to phase separate due to the topological constraint of the ring structure, as indicated by their higher $(\chi N)_{\text{ODT}}$. Furthermore, a direct disorder-to-cylinder transition window (f: 0.275–0.725) is observed in the phase diagram, which is significantly different from the mean field phase diagram of linear diblock copolymers. The domain spacing size ratio between cyclic and linear diblock copolymers is typically close to $1/\sqrt{2}$, indicating in segregation that a cyclic polymer with chain length N can be considered to be made up of a linear diblock with chain length $N/2$. Finally, cyclic diblock copolymers are strongly stretched along the direction perpendicular to the interface in phase-separated states.

ACKNOWLEDGMENTS

We thank Professor An-Chang Shi for illuminating discussions. This work was funded by the National Basic Research Program of China (Grant No. 2011CB605700) and National Natural Science Foundation of China (Grants Nos. 20990231 and 20874021).

[1] H. R. Kricheldorf, J. Polym. Sci., Part A: Polym. Chem. **48**, 251 (2010).
[2] M. Muller, J. P. Wittmer, and M. E. Cates, Phys. Rev. E **53**, 5063 (1996).
[3] S. Brown and G. Szamel, J. Chem. Phys. **108**, 4705 (1998).
[4] S. Brown and G. Szamel, J. Chem. Phys. **109**, 6184 (1998).

[5]K. Hur, R. G. Winkler, and D. Y. Yoon, Macromolecules **39**, 3975 (2006).
[6]V. Arrighi, S. Gagliardi, A. C. Dagger, J. A. Semlyen, J. S. Higgins, and M. J. Shenton, Macromolecules **37**, 8057 (2004).
[7]G. B. McKenna, G. Hadziioannou, P. Lutz, G. Hild, C. Strazielle, C. Straupe, P. Rempp, and A. J. Kovacs, Macromolecules **20**, 498 (1987); K. Ishizu and H. Kanno, Polymer **73**, 1487 (1996); B. Lepoittevin, M. Dourges, M. Masure, P. Hemery, K. Baran, and H. Cramail, Macromolecules **33**, 8218 (2000).
[8]J. Roovers, Macromolecules **21**, 1517 (1988).
[9]M. Antonietti, J. Coutandin, R. Grutter, and H. Sillescu, Macromolecules **17**, 798 (1984); P. J. Mills, J. W. Mayer, E. J. Kramer, G. Hadziioannou, P. Lutz, C. Strazielle, P. Rempp, and A. J. Kovacs, Macromolecules **20**, 513 (1987); S. F. Tead, E. J. Kramer, G. Hadziioannou, M. Antonietti, H. Sillescu, P. Lutz, and C. Strazielle, Macromolecules **25**, 3942 (1992).
[10]J. Roovers, Macromolecules **18**, 1359 (1985); L. Rique-Lurbet, M. Schappacher, and A. Deffieux, Macromolecules **27**, 6318 (1994); M. Schappacher and A. Deffieux, Macromolecules **34**, 5827 (2001); P. G. Santangelo, C. M. Roland, T. Chang, D. Cho, and J. Roovers, Macromolecules **34**, 9002 (2001); G. C. Nossarev and T. E. Hogen-Esch, Macromolecules **35**, 1604 (2002); R. Chen, X. Zhang, and T. E. Hogen-Esch, Macromolecules **36**, 7477 (2003).
[11]H. Durmaz, A. Dag, G. Hizal, and U. Tunca, J. Polym. Sci., Part A: Polym. Chem. **48**, 5083 (2010).
[12]J. F. Marko, Macromolecules **26**, 1442 (1993).
[13]H.-J. Qian, Z.-Y. Lu, L.-J. Chen, Z.-S. Li, and C.-C. Sun, Macromolecules **38**, 1395 (2005).
[14]W. H. Jo and S. S. Jang, J. Chem. Phys. **111**, 1712 (1999).
[15]S. Lecommandoux, R. Borsali, M. Schappacher, A. Deffieux, T. Narayanan, and C. Rochas, Macromolecules **37**, 1843 (2004).
[16]Y. Q. Zhu, S. P. Gido, H. Iatrou, N. Hadjichristidis, and J. W. Mays, Macromolecules **36**, 148 (2003).
[17]E. Minatti, R. Borsali, M. Schappacher, A. Deffieux, V. Soldi, T. Narayanan, and J. L. Putaux, Macromol. Rapid Commun. **23**, 978 (2002).
[18]E. Minatti, P. Viville, R. Borsali, M. Schappacher, A. Deffieux, and R. Lazzaroni, Macromolecules **36**, 4125 (2003).
[19]R. L. Lescanec, D. A. Hajduk, G. Y. Kim, Y. Gan, R. Yin, S. M. Gruner, T. E. Hogen-Esch, and E. L. Thomas, Macromolecules **28**, 3485 (1995).
[20]K. Ishizu and A. Ichimura, Polymer **39**, 6555 (1998).
[21]G. H. Fredrickson, *The Equilibrium Theory of Inhomogeneous Polymers* (Oxford University Press, Oxford, 2006).
[22]M. W. Matsen and M. Schick, Phys. Rev. Lett. **72**, 2660 (1994).
[23]F. Drolet and G. H. Fredrickson, Phys. Rev. Lett. **83**, 4317 (1999).
[24]A. Takano, O. Kadoi, K. Hirahara, S. Kawahara, Y. Isono, J. Suzuki, and Y. Matsushita, Macromolecules **36**, 3045 (2003).
[25]A. J. Ryan, S.-M. Mai, J. P. A. Fairclough, I. W. Hamley, and C. Booth, Phys. Chem. Chem. Phys. **3**, 2961 (2001).
[26]A. N. Morozov and J. G. E. M. Fraaije, Macromolecules **34**, 1526 (2001).
[27]A. Weyersbery and T. A. Vilgis, Phys. Rev. E **49**, 3097 (1994).